Stereodynamical Control of a Quantum Scattering Resonance in Cold Molecular Collisions

Pablo G. Jambrina[*]

Departamento de Química Física. Universidad de Salamanca, Salamanca 37008, Spain

James F. E. Croft[†]

*The Dodd-Walls Centre for Photonic and Quantum Technologies, Dunedin 9054, New Zealand and Department of Physics,
University of Otago, Dunedin 9054, New Zealand*

Hua Guo[‡]

Department of Chemistry and Chemical Biology, University of New Mexico, Albuquerque, New Mexico 87131, USA

Mark Brouard[§]

*The Department of Chemistry, University of Oxford, The Chemistry Research Laboratory,
Oxford OX1 3TA, United Kingdom*

Naduvalath Balakrishnan[‖]

Department of Chemistry and Biochemistry, University of Nevada, Las Vegas, Nevada 89154, USA

F. Javier Aoiz[¶]

Departamento de Química Física. Universidad Complutense. Madrid 28040, Spain

Cold collisions of light molecules are often dominated by a single partial wave resonance. For the rotational quenching of HD ($v = 1, j = 2$) by collisions with ground state *para*-H_2, the process is dominated by a single $L = 2$ partial wave resonance centered around 0.1 K. Here, we show that this resonance can be switched on or off simply by appropriate alignment of the HD rotational angular momentum relative to the initial velocity vector, thereby enabling complete control of the collision outcome.

DOI: 10.1103/PhysRevLett.123.043401

At cold (<1 K) and ultracold (<1 μK) temperatures molecules can be prepared in precisely defined quantum states and interrogated with unprecedented precision. Recent developments in molecule cooling and trapping technologies [1–8] as well as merged or co-expanding beam techniques [9–14] have made it increasingly possible to study molecular systems at these low temperatures. Such systems have even been used in the frontiers of particle physics [15], for example, in the search for the electric dipole moment of the electron [16–18]. Cold and ultracold molecules therefore offer an ideal platform on which to precisely study fundamental aspects of molecular dynamics [19–22] such as the role of quantum statistics [23], threshold laws [24], and geometric-phase effects [25].

One of the basic questions in molecular dynamics is the dependence of a collision outcome on the relative orientation and/or alignment of the colliding molecules—the stereodynamics of a collision process [26–34]. At cold and ultracold temperatures, where collisions proceed through just one or a few partial waves, their stereodynamics can be studied at the most fundamental level—the single quantum state level. In a recent series of papers Perreault *et al.* have

examined the role that the initial alignment of HD plays in cold collisions with H_2 and D_2 [35,36]. Control over rotational quenching rates was demonstrated, and subsequent theoretical studies revealed that for certain states the scattering dynamics of cold HD + o-H_2 collisions is determined by a single ($L = 2$) partial-wave shape resonance at around 1 K [37,38].

While the stereodynamics of atom-diatom collisions has been explored in previous theoretical studies [39–45], collisions between oriented and/or aligned molecules in cold conditions remain largely unexplored [46]. In this Letter, we apply theoretical methods to describe the stereodynamics of inelastic molecule-molecule collisions, specifically, to rotational quenching of HD in cold collisions with p-H_2. In particular, we demonstrate how the stereodynamics of cold molecule-molecule collisions can be determined by a single partial wave shape resonance and how it can be used to achieve exquisite control of the collision outcome.

Quantum mechanical (QM) inelastic scattering calculations were carried out using the time-independent coupled-channel formalism within the total angular momentum

(TAM) representation of Arthurs and Dalgarno [47], which has previously been successfully applied to collisions of H_2 with H_2 [48–50] and HD [51–53]. The scattering calculations were performed using a modified version of the TwoBC code [54,55] on the full-dimensional potential surface of Hinde [56]. In the TAM representation the rotational angular momenta of the dimers, $\boldsymbol{j}_{H_2}$ and $\boldsymbol{j}_{HD}$, are coupled to form $\boldsymbol{j}_{12} = \boldsymbol{j}_{H_2} + \boldsymbol{j}_{HD}$, which is in turn coupled with the orbital angular momentum $\boldsymbol{L}$ to form the total angular momentum $\boldsymbol{J} = \boldsymbol{L} + \boldsymbol{j}_{12}$. Scattering calculations are performed separately for each value of the total angular momentum J and parity $I = (-1)^{j_{H_2}+j_{HD}+L}$ that reflects the inversion symmetry of the wave function [57], yielding the scattering (S) matrix, $S^J_{\gamma,\gamma'}$, labeled by the asymptotic entrance and exit channels γ and γ', respectively (where $\gamma \equiv j_{HD}j_{H_2}Lj_{12}$). The state-to-state integral cross section (ICS) is given in terms of the S matrix by

$$\sigma_{\alpha\to\alpha'} = \frac{\pi}{k_\alpha^2} \frac{\sum_{\gamma,\gamma'}(2J+1)|\delta_{\gamma,\gamma'} - S^J_{\gamma,\gamma'}|^2}{(2j_{H_2}+1)(2j_{HD}+1)}, \qquad (1)$$

where α is the combined molecular state, $\alpha \equiv v_{H_2}j_{H_2}v_{HD}j_{HD}$, and k_α^2 is the square of the wave vector. From the S matrix, the scattering amplitudes $f_{\alpha'\Omega',\alpha\Omega}$ were determined using the procedure described in Ref. [37]. Ω (Ω') are the helicities, that is, the projection of j (j'), onto the approach (recoil) direction.

Inelastic collisions of HD ($v=1$, $j=2$) with $p\text{-}H_2(v=0$, $j=0$) at low collision energies are dominated by $\Delta j = -1$ and -2 transitions in HD leading to HD ($v'=1, j'=1$) + H_2 and HD ($v'=1, j'=0$) + H_2, respectively. Vibrational deexcitation of HD is energetically allowed, but the ICS for vibrational relaxation is around 5–6 orders of magnitude smaller at these collision energies. Energetically, two-quanta rotational excitation of $p\text{-}H_2$ is not allowed.

The energy dependence of the rotational quenching cross sections is shown in the top panel of Fig. 1. It is seen that at the lowest energies considered, the ICS for $\Delta j = -1$ is about a factor of 7 larger than for $\Delta j = -2$. Both show the onset of the Wigner threshold regime below ~ 0.01 K ($\propto E_{coll}^{-1/2}$ for pure s-wave collisions). The most salient feature for $\Delta j = -1$ is the presence of a sharp resonance at 0.1 K, where the ICS increases by almost a factor of 4. This is an $L = 2$ shape resonance that is caused by a single S-matrix element corresponding to $L = 2$ and $J = 3$ in the TAM representation. As a consequence of this, the resonance has a defined parity, in this case the block that does not include $\Omega = 0$, which as we will show later has important consequences for the collision mechanism. This particular resonance is not observed for $\Delta j = -2$, even though most of the scattering also comes from $L = 2$. Such resonances are ubiquitous features of inelastic and
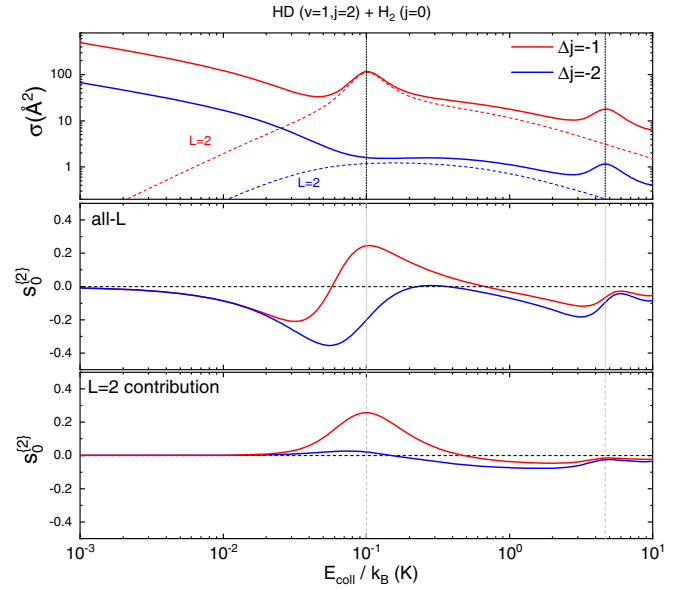

FIG. 1. Integral cross section for the HD ($v = 1, j = 2$) + H_2 ($v = 0, j = 0$) inelastic collisions as a function of the collision energy. Top panel: ICS for $\Delta j = -1$ (solid red line) and $\Delta j = -2$ (solid blue line). The contributions of the $L = 2$ partial wave to the ICS are shown as dashed lines. Middle and bottom panels: Energy dependence of the $s_0^{\{2\}}$ integral alignment moment for $\Delta j = -1$ (red) and -2 (blue). Middle panel shows the overall results and the $L = 2$ contribution is shown in the bottom panel.

reactive collisions, especially in the cold regime. Here we show how they can be used to reveal the collision mechanism and, perhaps more importantly, control the collision outcome.

The concept of a collision mechanism can be at times somewhat vague, relying on qualitative rather than on quantitative results, which can lead to misinterpretations. To avoid any ambiguities we use the three-vector correlation $\boldsymbol{k} - \boldsymbol{j}_{HD} - \boldsymbol{k}'$ (where $\boldsymbol{k}$ and $\boldsymbol{k}'$ define the approach and the recoil directions) which is especially well suited to characterizing collision mechanisms within a purely quantum-mechanical framework [58–60]. More explicitly we use the set of reactant polarization parameters $s_q^{\{k\}}$ of rank k and component $q = -k, \ldots, k$, which define the vector correlation [61]. The most relevant of these parameters is $s_0^{\{2\}}$, the first alignment moment of $\boldsymbol{j}$ about the incoming relative velocity. Negative values of $s_0^{\{2\}}$ indicate a preference for head-on collisions (rotational angular momentum $\boldsymbol{j}_{HD}$ perpendicular to $\boldsymbol{k}$), whereas positive values indicate a preference for side-on collisions ($\boldsymbol{j}_{HD}$ mostly parallel to $\boldsymbol{k}$). The polarization parameters are calculated from the integration of the polarization-dependent differential cross sections $S_q^{(k)}(\theta)$ over the scattering angle θ. For the $\boldsymbol{k} - \boldsymbol{j}_{HD} - \boldsymbol{k}'$ correlation the $S_q^{(k)}(\theta)$ can be determined from $f_{\alpha'\Omega',\alpha\Omega}$ [45]

$$S_q^{(k)}(\theta) = \frac{1}{(2j_{HD}+1)(2j_{H_2}+1)}$$
$$\times \sum_{\Omega_1 \Omega_2} \sum_{\delta} f_{\alpha'\delta,\alpha\Omega_1}[f_{\alpha'\delta,\alpha\Omega_2}]^* \langle j_{HD}\Omega_1, kq | j_{HD}\Omega_2 \rangle,$$
$$(2)$$

where $\langle .., .. | .. \rangle$ denotes the Clebsch-Gordan coefficient, and δ is the combined index $\delta \equiv \Omega_{H_2}\Omega'_{H_2}\Omega'_{HD}$.

The middle panel of Fig. 1 shows $s_0^{\{2\}}$ as a function of the collision energy for both the $\Delta j = -1$ and -2 transitions. At the lowest energies, the moment goes to zero, as required for ultracold collisions [46]. With increasing collision energy, $s_0^{\{2\}}$ takes negative values for both transitions, showing a preference for head-on encounters. However, at the proximity of the resonance, $s_0^{\{2\}}$ exhibits markedly different behavior for the two transitions. It turns positive for $\Delta j = -1$, peaking at the energy of the resonance (denoted with a vertical dashed line), while for $\Delta j = -2$ it remains negative. This shows that the resonance for $\Delta j = -1$ is associated with a specific mechanism that is not shared by the $\Delta j = -2$ transition. At energies above the resonance, $s_0^{\{2\}}$ again shows the same trend for both transitions, with a small change around 4.75 K caused by a second resonance (present in both Δj transitions) that does not change the mechanism significantly.

To unambiguously analyze the effect of the resonance, the $L = 2$ contribution to $s_0^{\{2\}}$ is shown in the bottom panel of Fig. 1. It is calculated by including only the $L = 2$ elements of the S matrix (without considering their coherences with other L values). Regardless of Δj, the $L = 2$ contribution to $s_0^{\{2\}}$ goes to zero at ultracold energies, as does $\sigma_{L=2}$. Moreover, up to 0.5 K, including the resonance, the sign of the $L = 2$ contribution to $s_0^{\{2\}}$ is positive (favoring side-on collisions) while it is negative for higher collision energies. Although at the resonance the sign of the $L = 2$ contribution to $s_0^{\{2\}}$ is positive for both $\Delta j = -1$ and -2, its magnitude is much larger for the former. Since $L = 2$ collisions dominate around 0.1 K for both Δj, these results indicate that the overall change of $s_0^{\{2\}}$, and hence of the collision mechanism, is caused by the resonance and not due to a larger contribution of $L = 2$.

The distinct mechanism for the resonance suggests that it might be possible to suppress its effect by appropriate state preparation of the HD rotational angular momentum [35,36]. The cross sections for different extrinsic preparations can be computed following the procedure described in Ref. [45]. If HD is prepared in a directed state, $m = 0$, where m is the magnetic quantum number, it leads to the alignment of the internuclear axis along the quantization axis (in the case of Refs. [35,36] the polarization vector of the pump and Stokes lasers). By varying the direction of the

laboratory-fixed axis with regard to the scattering frame it is possible to change the external preparations generating different relative geometries of the reactants prior to the collision. We will label the different extrinsic preparations using β and α, where β is the polar angle between the polarization vector and the initial relative velocity, and α is the azimuthal angle that defines the direction of the polarization vector with respect to the $k - k'$ frame. Accordingly, $\beta = 0°$, and $90°$ imply head-on and side-on collisions, respectively. The equation that relates the observed differential cross section (DCS) for a given preparation $(d\sigma_\alpha^\beta / d\omega)$ of the HD rotational angular momentum for unpolarized H_2 is [45]

$$\frac{d\sigma_\alpha^\beta}{d\omega} = \sum_{k=0}^{2j_{HD}} \sum_{q=-k}^{k} (2k+1)[S_q^{(k)}(\theta)]^* A_0^{(k)} C_{kq}(\beta, \alpha), \quad (3)$$

where $C_{kq}(\beta, \alpha)$ are the modified spherical harmonics, and the extrinsic moments $A_q^{(k)}$ define the preparation in the laboratory frame [45]. The ICS can be obtained by integrating $d\sigma_\alpha^\beta / d\omega$ over the scattering and the azimuthal angles, hence depending only on β.

Figure 2 shows the ICS for different experimentally achievable extrinsic preparations. The results for $\Delta j = -2$ are relatively featureless, and are identical to those shown in Ref. [38]. In the Wigner threshold regime, no control can be attained for the ICS [46]. With increasing collision energy, however, $\beta = 0°$ always leads to larger ICSs (by up to a factor of 2). The effect of $\beta = 90°$, and $\beta = $ mag (magic angle) preparations is milder, leading to only small changes in the ICSs with respect to the unpolarized case.
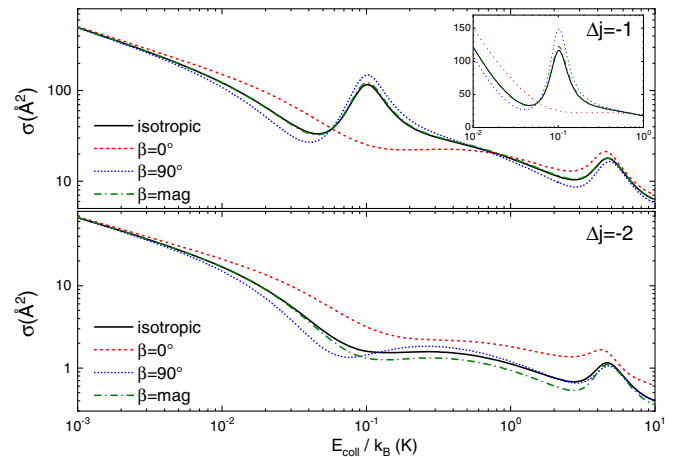

FIG. 2. Integral cross section as a function of the collision energy for $\Delta j = -1, -2$ for different preparations of the HD internuclear axis, $\beta = 0°$ (red line), $\beta = 90°$ (blue line), and the magic angle (olive line). The isotropic preparation (in the absence of external alignment) is shown in black. The inset shows the resonance region in a linear ordinate-axis scale.

For $\Delta j = -1$ the situation is similar for energies below the resonance. However, at the resonance the collision mechanism changes rather abruptly, and the $\beta = 0°$ preparation, which implies head-on collision, leads to a sudden decrease of the ICS, by close to a factor of 5, the most extreme effect that could be observed for any preparation of a sharp $j = 2$ state. Since the $\beta = 0°$ preparation is the same as collisions with $\Omega = 0$ exclusively, the fact that the S-matrix element that causes the resonance does not contain $\Omega = 0$ leads to the disappearance of the resonance.

Well above the resonance, at $E_{\mathrm{coll}} \geq 0.6$ K, the effect somewhat reverts back to the behavior observed below the resonance, with $\beta = 0°$ again leading to a slight increase in the ICS. To sum up, the alignment of $\mathbf{j}_{\mathrm{HD}}$ perpendicular to $\mathbf{k}$ slightly enhances the ICS except at the resonance, where it brings about the suppression of the resonance as if it were switched off. The effect of other preparations $\beta = 90°$ and $\beta = \mathrm{mag}$ is relatively minor and, apparently, does not affect the resonance significantly, as far as the ICS is concerned.

Up to this point, we have shown that at the resonance there is a change in the collision mechanism, which can be used to control the ICS by changing the preparation of the HD rotational angular momentum. It has been demonstrated recently by Perreault *et al.* that it is possible to determine the DCS for different reagent preparations [35,36], so we now shift our attention to investigating how the DCS is affected by state preparation of the HD molecule. Figure 3 shows the DCS as a function of the scattering angle and collision energy for $\Delta j = -1$. The isotropic DCS (with unpolarized collision partners) is shown in panel (a), which features a slight preference for forward scattering. In particular, the resonance appears as a sharp "ridge" with a clear preference for forward scattering. For $\beta = 0°$, panel (b), the situation is completely different. First, the resonance completely vanishes, and at 0.1 K there are no marked changes or discontinuities in the energy dependence of the DCS. In addition, the shape of the DCS displays prominent forward and backward peaks irrespective of the collision energy. At low collision energies there is a third peak in the DCS that only survives for energies below 0.03 K. There is also a resonance around $E_{\mathrm{coll}} \sim 5$ K, which unlike the 0.1 K resonance is slightly enhanced by this external preparation.

While the $\beta = 90°$ and $\beta = \mathrm{mag}$ preparations have a minor effect on the ICS, the polarization of $\mathbf{j}_{\mathrm{HD}}$ has a dramatic effect on the shape of the DCS. Figures 3(c)–3(f) show the effect of $\beta = 90°$ and $\beta = \mathrm{mag}$ and $\alpha = 0°$, 180° preparations on the DCS. The shape and magnitude of the DCS for all these cases differ from each other and from the isotropic case. Moreover, all of them show distinct features at the resonance. For $\beta = 90°$, $\alpha = 0, 90°$, the DCS at the resonance has two prominent peaks at around 30° and 150°, while for $\beta = \mathrm{mag}$ and $\alpha = 0°$ there is a strong enhancement of forward scattering at the resonance. While for all nonzero β values the resonance at 0.1 K is present, its angular
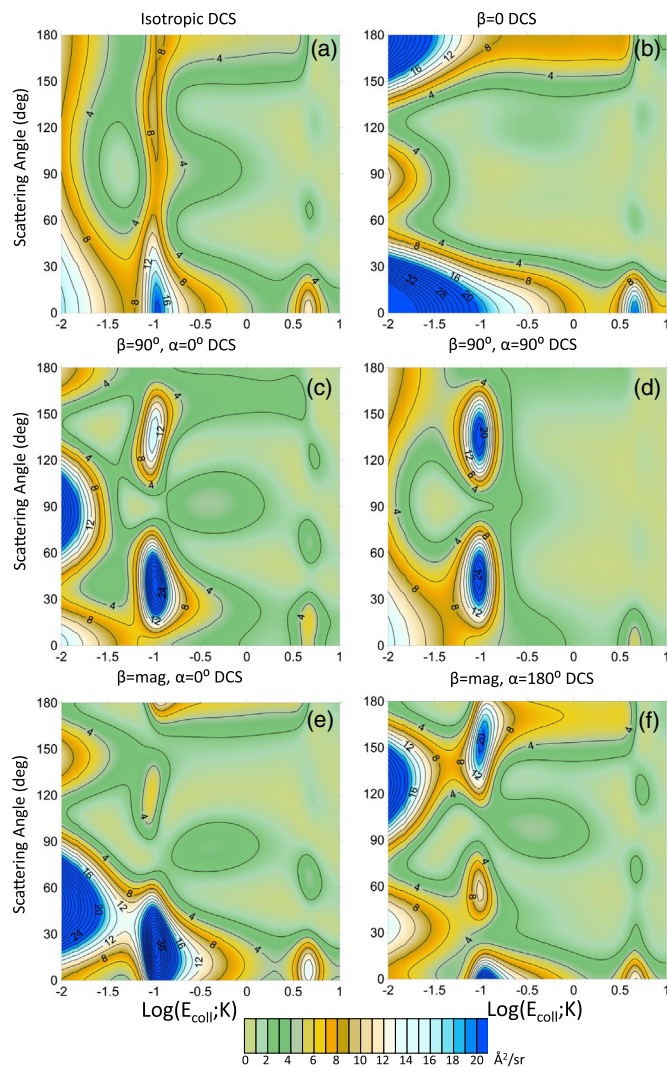

FIG. 3. Contour plots showing the collision energy dependence of the DCS for the $\Delta j = -1$ transition with different preparation of the HD rotational angular momentum. The effect of the resonance is prominent for all preparations except for $\beta = 0$, for which the resonance disappears. Log(E_{col}; K) refers to Log($E_{\mathrm{coll}}/E_{\mathrm{ref}}$) where $E_{\mathrm{ref}} = k_B$ 1 K. $S_0^{\{2\}}(\theta)$ for four representative energies are shown in the Supplemental Material [62].

distribution is exquisitely sensitive to β and α, showing that the resonance can be used to control not just the magnitude of the ICS, but also the scattering direction [32]. This provides a powerful tool to elucidate the sterodynamics of resonance-mediated collisions and fine-tune calculated interaction potentials against controlled experiments.

To gain further insight into the reaction mechanism we analyze the remaining polarization parameters besides $s_0^{\{2\}}$. For initial $j = 2$, eight independent parameters contribute to the alignment of the internuclear axis distribution, depicted as "stereodynamical portraits" [63,64] for a given polarization of the rotational angular momentum. These are 3D plots showing the probability density function of the HD internuclear axis leading to a specific state. Figure 4
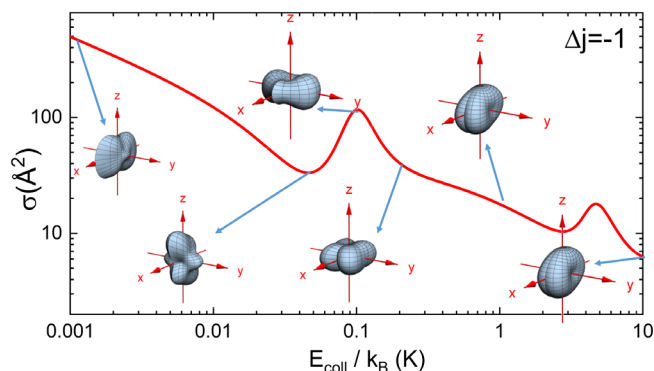
FIG. 4. Integral cross section as a function of the collision energy for $\Delta j = -1$ along with the internuclear axis stereo-dynamical portraits. The reference frame is defined by the reactants approach ($\mathbf{k}$) and the products recoil ($\mathbf{k}'$) directions. The z axis is parallel to $\mathbf{k}$, the x-z plane is the scattering plane, and the y axis is parallel to $\mathbf{k} \times \mathbf{k}'$.

presents the stereodynamical portraits associated with the internuclear axis of HD for $\Delta j = -1$. At 10^{-3} K, the HD internuclear axis is contained in the scattering plane, although it does not show a significant preference towards head-on or side-on encounters. Just below the resonance it starts to show a strong preference towards head-on collisions (typically associated with small impact parameters). A sudden change of the mechanism occurs at the resonance, with a clear preference for side-on encounters (internuclear axis perpendicular to z). Just above the resonance the internuclear axis remains perpendicular to the approach direction, but preferentially contained in the xy plane. With increasing collision energy, the internuclear axis is no longer aligned along or perpendicular to z.

Altogether, these results demonstrate that, in the cold-energy regime, inelastic collisions between HD ($v = 1$, $j = 2$) and p-H_2 are controlled by a resonance at 0.1 K that causes profound changes to the reaction mechanism that favors side-on collisions, typically associated with large impact parameters, over head-on collisions that would have been preferred if the resonance were absent. This sudden change in mechanism permits exquisite control of the collision outcome by using different preparations of the HD internuclear axis, and makes it possible to switch off the resonance altogether. The effect of the initial HD alignment becomes most evident in the DCS, which changes dramatically for the alternative preparations investigated. Energy resolved measurements of state-resolved angular distributions of HD in collisions with p-H_2 would be desirable to validate these predictions. Our findings can be generalized to other systems and, indeed, some degree of control may be expected for other resonances in the cold regime.

[*] pjambrina@usal.es
[†] j.croft@otago.ac.nz
[‡] hguo@unm.edu
[§] mark.brouard@chem.ox.ac.uk
[‖] naduvala@unlv.nevada.edu
[¶] aoiz@quim.ucm.es

[1] R. Wynar, R. S. Freeland, D. J. Han, C. Ryu, and D. J. Heinzen, Science **287**, 1016 (2000).
[2] C. A. Regal, C. Ticknor, J. L. Bohn, and D. S. Jin, Nature (London) **424**, 47 (2003).
[3] B. C. Sawyer, B. L. Lev, E. R. Hudson, B. K. Stuhl, M. Lara, J. L. Bohn, and J. Ye, Phys. Rev. Lett. **98**, 253002 (2007).
[4] E. S. Shuman, J. F. Barry, and D. DeMille, Nature (London) **467**, 820 (2010).
[5] M. T. Hummon, M. Yeo, B. K. Stuhl, A. L. Collopy, Y. Xia, and J. Ye, Phys. Rev. Lett. **110**, 143001 (2013).
[6] N. Akerman, M. Karpov, Y. Segev, N. Bibelnik, J. Narevicius, and E. Narevicius, Phys. Rev. Lett. **119**, 073204 (2017).
[7] L. Anderegg, B. L. Augenbraun, E. Chae, B. Hemmerling, N. R. Hutzler, A. Ravi, A. Collopy, J. Ye, W. Ketterle, and J. M. Doyle, Phys. Rev. Lett. **119**, 103201 (2017).
[8] S. Truppe, H. Williams, M. Hambach, L. Caldwell, N. Fitch, E. Hinds, B. Sauer, and M. Tarbutt, Nat. Phys. **13**, 1173 (2017).
[9] A. B. Henson, S. Gersten, Y. Shagam, J. Narevicius, and E. Narevicius, Science **338**, 234 (2012).
[10] J. Jankunas, B. Bertsche, K. Jachymski, M. Hapka, and A. Osterwalder, J. Chem. Phys. **140**, 244302 (2014).
[11] A. Klein, Y. Shagam, W. Skomorowski, P. S. Żuchowski, M. Pawlak, L. M. Janssen, N. Moiseyev, S. Y. van de Meerakker, A. van der Avoird, C. P. Koch et al., Nat. Phys. **13**, 35 (2017).
[12] W. E. Perreault, N. Mukherjee, and R. N. Zare, Chem. Phys. **514**, 150 (2018).
[13] C. Amarasinghe and A. G. Suits, J. Phys. Chem. Lett. **8**, 5153 (2017).
[14] C. Naulin and M. Costes, Int. Rev. Phys. Chem. **33**, 427 (2014).
[15] D. DeMille, J. M. Doyle, and A. O. Sushkov, Science **357**, 990 (2017).
[16] J. J. Hudson, D. M. Kara, I. Smallman, B. E. Sauer, M. R. Tarbutt, and E. A. Hinds, Nature (London) **473**, 493 (2011).
[17] J. Baron, W. C. Campbell, D. DeMille, J. M. Doyle, G. Gabrielse, Y. V. Gurevich, P. W. Hess, N. R. Hutzler, E. Kirilov, I. Kozyryev, B. R. O'Leary, C. D. Panda, M. F. Parsons, E. S. Petrik, B. Spaun, A. C. Vutha, and A. D. West, Science **343**, 269 (2014).

[18] W. B. Cairncross, D. N. Gresh, M. Grau, K. C. Cossel, T. S. Roussy, Y. Ni, Y. Zhou, J. Ye, and E. A. Cornell, Phys. Rev. Lett. **119,** 153001 (2017).

[19] M. T. Bell and T. P. Softley, Mol. Phys. **107,** 99 (2009).

[20] L. D. Carr, D. DeMille, R. V. Krems, and J. Ye, New J. Phys. **11,** 055049 (2009).

[21] N. Balakrishnan, J. Chem. Phys. **145,** 150901 (2016).

[22] J. L. Bohn, A. M. Rey, and J. Ye, Science **357,** 1002 (2017).

[23] S. Ospelkaus, K.-K. Ni, D. Wang, M. H. G. de Miranda, B. Neyenhuis, G. Quéméner, P. S. Julienne, J. L. Bohn, D. S. Jin, and J. Ye, Science **327,** 853 (2010).

[24] N. Balakrishnan and A. Dalgarno, Chem. Phys. Lett. **341,** 652 (2001).

[25] B. K. Kendrick, J. Hazra, and N. Balakrishnan, Phys. Rev. Lett. **115,** 153201 (2015).

[26] R. B. Bernstein, D. R. Herschbach, and R. D. Levine, J. Phys. Chem. **91,** 5365 (1987).

[27] R. D. Levine and R. B. Bernstein, *Molecular Reaction Dynamics and Chemical Reactivity* (Oxford University Press, Oxford, 1987).

[28] A. J. Orr-Ewing and R. N. Zare, Annu. Rev. Phys. Chem. **45,** 315 (1994).

[29] A. J. Orr-Ewing, J. Chem. Soc., Faraday Trans. **92,** 881 (1996).

[30] F. J. Aoiz, M. Brouard, S. D. S. Gordon, B. Nichols, S. Stolte, and V. Walpole, Phys. Chem. Chem. Phys. **17,** 30210 (2015).

[31] T. R. Sharples, J. G. Leng, T. F. M. Luxford, K. G. McKendrick, P. G. Jambrina, F. J. Aoiz, D. W. Chandler, and M. L. Costen, Nat. Chem. **10,** 1148 (2018).

[32] C. G. Heid, V. Walpole, M. Brouard, P. G. Jambrina, and F. J. Aoiz, Nat. Chem. **11,** 662 (2019).

[33] F. Wang, K. Liu, and P. Rakitzis, Nat. Chem. **4,** 636 (2012).

[34] F. Wang, J.-S. Lin, and K. Liu, J. Chem. Phys. **140,** 084202 (2014).

[35] W. E. Perreault, N. Mukherjee, and R. N. Zare, Science **358,** 356 (2017).

[36] W. E. Perreault, N. Mukherjee, and R. N. Zare, Nat. Chem. **10,** 561 (2018).

[37] J. F. E. Croft, N. Balakrishnan, M. Huang, and H. Guo, Phys. Rev. Lett. **121,** 113401 (2018).

[38] J. F. E. Croft and N. Balakrishnan, J. Chem. Phys. **150,** 164302 (2019).

[39] M. P. de Miranda and D. C. Clary, J. Chem. Phys. **106,** 4509 (1997).

[40] S. A. Kandel, A. J. Alexander, Z. H. Kim, R. N. Zare, F. J. Aoiz, L. Bañares, J. F. Castillo, and V. S. Rábanos, J. Chem. Phys. **112,** 670 (2000).

[41] P. G. Jambrina, J. Aldegunde, F. J. Aoiz, M. Sneha, and R. N. Zare, Chem. Sci. **7,** 642 (2016).

[42] J. Aldegunde, F. Javier Aoiz, and M. P. de Miranda, Phys. Chem. Chem. Phys. **10,** 1139 (2008).

[43] P. G. Jambrina, M. Menéndez, A. Zanchet, E. Garcia, and F. J. Aoiz, Phys. Chem. Chem. Phys. **21,** 14012 (2019).

[44] M. Brouard, H. Chadwick, C. J. Eyles, B. Hornung, B. Nichols, F. J. Aoiz, P. G. Jambrina, and S. Stolte, J. Chem. Phys. **138,** 104310 (2013).

[45] J. Aldegunde, M. P. de Miranda, J. M. Haigh, B. K. Kendrick, V. Sáez-Rábanos, and F. J. Aoiz, J. Phys. Chem. A **109,** 6200 (2005).

[46] J. Aldegunde, J. M. Alvarino, M. P. de Miranda, V. Saez Rabanos, and F. J. Aoiz, J. Chem. Phys. **125,** 133104 (2006).

[47] A. M. Arthurs and A. Dalgarno, Proc. R. Soc. A **256,** 540 (1960).

[48] J. Schaefer and W. Meyer, J. Chem. Phys. **70,** 344 (1979).

[49] S. K. Pogrebnya and D. C. Clary, Chem. Phys. Lett. **363,** 523 (2002).

[50] G. Quéméner, N. Balakrishnan, and R. V. Krems, Phys. Rev. A **77,** 030704(R) (2008).

[51] J. Schaefer, Astron. Astrophys. Suppl. Ser. **85,** 1101 (1990).

[52] D. R. Flower, J. Phys. B **32,** 1755 (1999).

[53] N. Balakrishnan, J. F. E. Croft, B. H. Yang, R. C. Forrey, and P. C. Stancil, Astrophys. J. **866,** 95 (2018).

[54] R. Krems, TwoBC—quantum scattering program, University of British Columbia, Vancouver, Canada, 2006.

[55] G. Quéméner and N. Balakrishnan, J. Chem. Phys. **130,** 114303 (2009).

[56] R. J. Hinde, J. Chem. Phys. **128,** 154308 (2008).

[57] M. H. Alexander and A. E. DePristo, J. Chem. Phys. **66,** 2166 (1977).

[58] F. J. Aoiz and M. P. de Miranda, in *Tutorials in Molecular Reaction Dynamics*, edited by M. Brouard and C. Vallance (RSC Publishing, Cambridge, 2010).

[59] D. A. Case and D. R. Herschbach, Mol. Phys. **30,** 1537 (1975).

[60] J. D. Barnwell, J. G. Loeser, and D. R. Herschbach, J. Phys. Chem. **87,** 2781 (1983).

[61] J. Aldegunde, M. P. de Miranda, J. M. Haigh, B. K. Kendrick, V. Saez-Rabanos, and F. J. Aoiz, J. Phys. Chem. A **109,** 6200 (2005).

[62] See Supplemental Material at http://link.aps.org/supplemental/10.1103/PhysRevLett.123.043401 for figure showing the renormalized intrinsic polarization dependent differential cross section $s_0^{\{2\}}$ calculated at four different energies.

[63] M. P. de Miranda and F. J. Aoiz, Phys. Rev. Lett. **93,** 083201 (2004).

[64] M. P. de Miranda, F. J. Aoiz, V. Sáez-Rábanos, and M. Brouard, J. Chem. Phys. **121,** 9830 (2004).